IEEE Access
Multidisciplinary ⋮ Rapid Review ⋮ Open Access Journal

Received February 4, 2020, accepted February 16, 2020, date of publication February 24, 2020, date of current version March 3, 2020.

Digital Object Identifier 10.1109/ACCESS.2020.2975805

WGM-Based Sensing of Characterized Glucose-Aqueous Solutions at mm-Waves

ALA ELDIN OMER[1,2,3], (Student Member, IEEE), SUREN GIGOYAN[1], GEORGE SHAKER[1,2,3], (Senior Member, IEEE), AND SAFIEDDIN SAFAVI-NAEINI[1,2], (Life Fellow, IEEE)

[1]Centre for Intelligent Antenna and Radio Systems (CIARS), University of Waterloo, Waterloo, ON N2L 3G1, Canada
[2]Department of Electrical and Computer Engineering, University of Waterloo, Waterloo, ON N2L 3G1, Canada
[3]Wireless Sensors and Devices Lab, Schlegel-University of Waterloo Research Institute for Aging, Waterloo, ON N2J 0E2, Canada

Corresponding author: Ala Eldin Omer (aeomomer@uwaterloo.ca)

This work was supported in part by the Natural Sciences and Engineering Research Council (NSERC), in part by the NSERC CREATE grant for training in Global Biomedical Technology Research and Innovation, in part by the C-COM Satellite Systems Inc., and in part by the Schlegel-University of Waterloo Research Institute of Aging (UW-RIA).

ABSTRACT A newly-developed commercial coaxial probe kit (DAK-TL) is used to characterize the electromagnetic properties of glucose-loaded samples prepared at a range of concentrations 0.7–1.2 mg/ml similar to Type-2 normal diabetics in a broad range of frequencies from 300 MHz to 67 GHz using two different 50 Ω open-ended coaxial probes. The objective is to determine the spectrum portion of the most sensitivity to slight variations in glucose concentrations and to identify the amount of change in the dielectric permittivity and loss tangent due to different concentrations of interest. The millimeter-wave range 50–67 GHz has shown to be promising for acquiring both high sensitivity and sufficient penetration depth for the most interaction between the glucose molecules and electromagnetic waves. Subsequently, the relative permittivity of the glucose-water mimicking samples are modeled in this mm-wave band using a single-pole Debye model with independent coefficients. The fitted Debye model is used to design a simple low-cost highly-sensitive integrated mm-wave sensing structure that utilizes the travelling-wave Whispering Gallery Modes (WGMs) launched in a dielectric disc resonator (DDR) when coupled to a dielectric image waveguide (DIG). The proposed sensor is used for continuous monitoring of glucose levels in blood mimicking aquatic solutions by tracking the variations in the magnitude and phase of the WGM transmission resonances in the mm-wave spectrum. This happens in reaction to the strong interactions of the coupled WGM evanescent field with the glucose samples loaded on top of the DDR inside a container. The sensor exhibits a high sensitivity performance (2.5–7.7 dB/[mg/ml]) for the two proposed DIG layouts, straight and curved, at the lower-order modes WGH_{600} and WGH_{700} of its five pure WGH modes supported in the frequency range 50–70 GHz as demonstrated by numerical simulations in a 3D full-wave EM solver and validated through proof-of-concept measurements.

INDEX TERMS Debye model, dielectric characterization, mm-wave sensing, non-invasive glucose detection, WGM resonator.

I. INTRODUCTION

Millimeter(mm)-wave frequencies have shown to be promising in developing various biomedical appliances due to the privileges they offer in terms of the enhanced security, available spectrum, reduced interference, and miniaturized sizing for fabricated devices [1]. The higher spatial resolution than microwaves, better sensitivity to the lossy water content, and less sensitivity to water contaminants; are all features that qualify the mm-wave for in-depth investigations by researchers to promote portable devices for sensing glucose concentrations [2]. This is becoming particularly important as diabetics need to continually monitor their blood glucose levels in order to meet certain glycemic targets and control it accordingly through remedies to avoid the susceptibility of any serious health complications like heart disease, stroke, coma, kidney failure, blindness, etc. [3]. Furthermore, hyperglycemia (>2.3 mg/ml) and hypoglycemia (<0.65 mg/ml)

The associate editor coordinating the review of this manuscript and approving it for publication was Boxue Du.

become avoidable situations if the glucose level is continuously monitored and controlled as required [4]. To meet the glycemic targets, patients of Type-1 should check up their blood glucose level in accordance with the insulin intake (four times a day), while Type-2 patients should check twice a day as recommended by the Canadian Diabetes Association [4]. Typical glucose levels in humans' blood for Type-2 diabetes vary in the range from 0.72 to 1.4 mg/ml before having a meal and should be less than 1.8 mg/ml within 1–2 hours after a meal [5]. The customary method used at home to check their blood glucose is through a glucometer device, where a blood sample is taken from the fingertip on a paper strip then inserted into the measurement device for a glucose reading [6]. This finger-pricking method is painful, invasive, and costly to the users who must prick their finger multiple times a day to draw blood for numerous measurements. Additionally, the infected paper strips and needles should be discarded and replaced with a fresh supply of test papers to analyze the subsequent samples.

To overcome these limitations and discomforts, researchers have conducted thorough investigations over the last decade on alternative blood glucose detection methods where different technologies have been applied including the optical techniques [7], [8], absorbance spectroscopy [9], [10], enzyme-based electrochemical methods that measure the external bodily fluids such as saliva [11], sweat [12], and tears [13], and correlate their glucose content to the glycemia in bloodstream. The radiofrequency (RF)/microwave sensing techniques have also been widely investigated to measure and correlate the EM properties of blood in superficial vessels to the glycemic level [14]–[18]. Measurements of the dielectric properties of blood biological tissues at subjective glucose concentrations similar to diabetes is essentially important for developing an accurate non-invasive microwave sensor for monitoring blood glucose levels. The microwave resonators are attractive tools that offer a great advantage for measuring the complex permittivity for tested liquids in narrow bands with a flexibility in design and fabrication process that is both simple and cost-effective. Additionally, these resonators feature the non-invasive measurements in non-destructive fashion that would not alter the tested samples by chemical or mechanical procedures [19].

Featured dielectric waveguides emerge as a reasonable substitute to overcome the limitations of the traditional metallic waveguides in manufacturing inaccuracies and conductive losses at mm-wave frequencies and beyond. They offer low-cost, low-loss and high confinement wave transmission inside whispering gallery mode (WGM) resonators that demonstrate high sensing capabilities with a higher sensitivity compared to the electrochemical, reflectometry, and quasi-optical methods [20]. Such resonators are not only favored for their high Q-factor resonances, but also for having relatively large size (in terms of wavelength) which makes their fabrication process a bit handy and tolerant to fabrication dimensional errors compared to the conventional dielectric resonators of lower-order modes [21]. The principle of operation for those resonance structures can be explicated by the evanescent field concept of interaction. WGMs are high-order modes characterized by the unique field distribution inside a dielectric disk/ring resonator (DDR/DRR) where most of the energy is confined towards the resonator boundaries [22]. Subsequently, the resonance characteristics of the DDR become quite sensitive to any small perturbation close to its boundary region rendering the resonator capable of differentiating various materials with very small differences in EM properties.

In this study, we propose a reliable low-cost mm-wave integrated WGM-based glucose bio-sensor that consists of a dielectric disc resonator (DDR) coupled to a dielectric image waveguide (DIG) with both combined inside a rectangular metallic waveguide. The proposed sensor aims at monitoring the glucose level in blood-like water-based solutions on a non-contact continuous manner in the mm-wave regime. The sensor operates based on the intensive interaction between the lossy glucose sample loaded on top of the DDR and the WGM evanescent field that is strongly coupled towards the boundaries of the loaded glucose sample. Therefore, the tiny variances in the dielectric properties of various glucose concentrations are detected in the sensor transmission response in terms of traceable variations in the S_{21} magnitude and phase at the WGM resonances. Towards such a design, we first measured the complex permittivity of assorted binary glucose-water solutions prepared at (0.7–1.2 mg/ml) considering the practical glycemic range of Type-2 normal diabetes, over the frequency spectrum from 300 MHz up to 67 GHz using a commercial coaxial probe kit (DAK-TL). This is done to locate the frequency portion that is most responsive to slight variations in glucose concentrations, and to identify the amount of change in the dielectric properties due to different concentrations of interest. Following this study, the proposed sensor was designed to operate in the mm-wave band (50–70 GHz) that exhibits higher sensitivity to variations in glucose levels by having the most interaction between the glucose molecules and EM waves. The measured dielectric parameters in the mm-wave band were fitted to a single-pole Debye model then used to analyze the scattering effect of the lossy blood mimicking solutions at disparate glucose levels using a high frequency numerical simulator by integrating the corresponding dielectric properties with the sensor at the frequency of interest. This is done to optimally design the WGM-based sensor and analyze its sensitivity performance at the different supported WGM modes when loaded with glucose samples of various concentrations.

This work is an initial step toward the goal of modeling human blood for a continuous monitoring. Figure. 1 illustrates one possible realization of the measurement setup for continuous blood glucose monitoring from the fingertip of a diabetes patient. The vector network analyzer (VNA) acquires the transmission measurements continuously from the WGM sensor and simultaneously forwards the measurement data to a computer connected via the GRIP cable where the RF measurements are analyzed and correlated to their

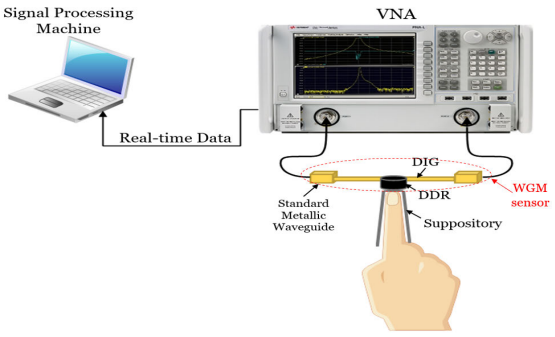

FIGURE 1. The potential of the proposed sensor for continuous glucose monitoring and the measurement setup.

accurate blood glucose concentrations using signal processing and machine learning algorithms.

The next sections in this paper are organized as follows: Section II discusses the generic model for the dielectric properties of glucose aqueous solutions and the research efforts for characterization in the mm-wave band. Section III presents the spectroscopy dielectric measurements for glucose solutions using the DAK-TL system. The proposed glucose sensing approach based on the WGM resonance perturbation is explained in Section IV, and the mathematical sensitivity analysis of WGM for glucose dielectric properties is presented in Section V. The design specification, numerical simulations, and in-vitro measurements for the proposed WGM glucose sensor are detailed in Section VI. Section VII presents a comprehensive discussion for the study findings as well as the comparison of the sensitivity performance to other state-of-art sensors. Section VIII concludes the paper and outlines the future work.

II. DIELECTRIC PROPERTIES OF GLUCOSE-LOADED SOLUTIONS AT MM-WAVES

For preliminary investigations on non-invasive glucose detection using RF sensors, aqueous glucose solutions can be utilized in the RF experiments to mimic blood samples at disparate glucose concentrations and assure the repeatability of the collected measurements. This approximation is valid as water contributes a high percentage (≈50%) of the entirety volume of human blood that contains other vital constituents at different proportions (e.g. glucose, Na, Ca, K, Cl, etc.) [23]. Generally speaking, lossy tissues of high-water contents (e.g. blood, aqueous solutions, etc.) are dispersive media where the EM properties depend on frequency as given in (1) that defines the relative complex permittivity for aqueous solutions of lossy nature as a function of the angular frequency $\omega = 2\pi f$ and the concentration ξ of any hydrophilic substance. This frequency dependency is mathematically described using the Debye Relaxation Model [24]

$$\epsilon_r(\omega, \xi) = \epsilon_r'(\omega, \xi) - j\epsilon_r''(\omega, \xi) \tag{1}$$

where the real part ϵ_r' is the dielectric constant (dielectric permittivity) that indicates the stored energy in the material when exposed to an external electric-field, and the imaginary part ϵ_r'' is the dielectric loss (loss factor) that is related to total attenuated and absorbed energy inside the material due to ionic conduction $\epsilon_{r\sigma}''$ and dipole rotation ϵ_{rd}'' loss mechanisms [25].

$$\epsilon_r''(\omega, \xi) = \epsilon_{rd}'' + \epsilon_{r\sigma}'' = \epsilon_{rd}''(\omega, \xi) + \frac{\sigma}{\omega\epsilon_o} \tag{2}$$

where σ is the ionic conductivity of the material in S/m and ϵ_o is the reference free-space permittivity (8.854×10^{-12} F/m).

The ratio between dissipated and stored energy in the material is labeled as loss tangent (dissipation factor) and given by

$$\tan\delta = \epsilon_r''/\epsilon_r' \tag{3}$$

The literature is not well-established with measurements that address the EM behavior of glucose liquid materials in higher frequencies in contrast to lower frequency ranges up to 10 GHz [5]. In fact, measurements in such high frequencies are challenged by the strict tolerances in manufacturing the RF measuring tools that often require very high accuracy, and hence their deployment in large-scale would be very expensive. A few researches, however, have focused on extracting the permittivity parameters for liquid samples of relatively high glucose concentrations at higher frequency ranges. For instance, the authors in [26] used different reflection and transmission sensing approaches to collect the permittivity measurements for aqueous glucose solutions of 1.5–5.0 mg/ml in a frequency range up to 40 GHz. The 50–75 GHz band was investigated in [27] for measuring the reflection coefficients using saline solutions of 5.0–30 mg/ml. The correlation between the reflected scattering coefficients and these concentrations was not sufficiently strong even for the high concentrations. In comparison, for measurements in the same band, a clear linear correlation was demonstrated in [5] between the transmitted EM energy in this mm-wave band and the glucose concentrations dissolved in watery and salty solutions. Two open-ended V-band waveguides (WR-15) connected to a VNA were used to measure the dielectric properties, reflection (S_{11}) and transmission (S_{21}) coefficients. The tested samples were prepared in a clinically relevant range of glucose concentrations (0.25–50 mg/ml). The scattering data of the transmission mode achieved better results compared to those collected in the reflection mode especially in the 59–64 GHz and 69–73 GHz frequency ranges. Another study [28] over the frequency range (28–93 GHz) used the mm-wave spectroscopy in reflection mode to detect sugar in watery solutions, blood imitators (physiological solution: 0.9% NaCl in water), and blood. The sensitivity of the extracted dielectric properties to glucose content was investigated for concentrations in the range 5.0–50 mg/ml. In [17] a waveguide transmission probe was clamped onto the ear of a live anesthetic rat in order to observe the EM properties continuously on VNA. The authors recorded a correlation between blood glucose concentrations

and the absorption/reflection properties of the mm-wave transmitted in the Ka band (27–40 GHz) as demonstrated by the considerable changes in the absorption/reflection parameters during the 0.5 mL intraperitoneal (IP) injection of glucose and insulin into the rat under experiment. A recent study in [29] proposed a mm-wave sensing system that consists of a pair of 60 GHz microstrip patch antennas placed across the interrogated blood sample. Measurements of the transmission coefficients were shown to be highly affected by changes in the permittivity along the signal path due to variations in glucose concentrations. Another interesting study in [30] proposed a novel sensing approach for glucose level monitoring using a 60 GHz mm-wave radar system. The proposed radar mechanism has shown greater capabilities for remote detection of blood glucose inside test tubes through detecting minute changes in their dielectric properties. The reflected mm-wave signals from the blood samples were analyzed using signal processing techniques to identify disparate glucose concentrations in the range 0.5–3.5 mg/ml and correlate them to the reflected mm-wave readings.

III. SPECTROSCOPY DIELECTRIC MEASUREMENTS OF GLUCOSE USING DAK-TL

Following up the aforementioned efforts, in this study, we investigated which frequency band could be of the most sensitivity to glucose level changes in the tested liquid specimens while understanding their dielectric behavior as reflected by the corresponding spectroscopy measurements. For this purpose, we used the updated software version of the DAK-TL (2.4.1.144) system to measure the EM dielectric properties of water-based glucose-loaded samples of concentrations (0.7–1.2 mg/ml) in four distinct frequency bands. DAK-TL is a fully-automated and software-controlled measuring tool that is used to precisely measure the dielectric properties of liquids available in small volumes (5–50 ml). It is based upon the open-ended coaxial probe technique commonly used for non-destructive sensing where the coaxial probe is pressed against a sample and the reflection coefficient is measured. The dielectric parameters of the sample under test (SUT) are then calculated from the reflection coefficient, the probe dimensions (diameters, bead permittivity), and the sample thickness. DAK-TL uses a precise and fast numerical algorithm that is capable of solving the improper integrals of complex functions and the equation inverse. This key algorithm is based on the equations formulated in [31] by Baker-Jarvis *et al*, and is run simultaneously while acquiring the S-parameters in order to calculate and plot the dielectric measurements in real time during the continuous sweep process.

A. SAMPLE PREPARATION

The tested samples of aqueous solutions were first prepared precisely using a micropipette device in a laboratory with disparate glucose concentrations 0.7, 0.8, 0.9, 1.0, 1.1, and 1.2 *mg/ml*. The dilution equation $C_1V_1 = C_2V_2$ was used to calculate the volume V_1 added from the standard glucose solution of $C_1 = 10\ mg/ml$, to achieve the desired concentrations for the prepared samples of volume $V_2 = 20\ ml$. The glucose concentrations of these samples were confirmed by testing a hemoglobin-mixed (or fake blood) version of these samples on a reference glucometer device. First, a 1:1 ratio was used to prepare these mixed solutions, thereby the glucometer reading should be half of the original concentrations. However, glucometer readings were much higher than expected as a result of testing concentrations at the very low end of the dynamic range of the glucometer. Alternatively, the relative amount of blood glucose in the test solution was increased using a 3:2 glucose solution to fake blood resulting into right expectations for the values of the measured concentrations as listed in Table. 1 for all the concentration readings of the prepared glucose-water samples using the reference glucometer device.

TABLE 1. Glucometer readings for the prepared samples.

Sample concentration (mg/ml)	Glucometer reading (mg/ml)	
	(1:1 ratio)	(3:2 ratio)
0.7	0.93	0.83
0.8	1.14	0.95
0.9	1.34	1.03
1.0	1.6	1.06
1.1	1.84	1.08
1.2	1.86	1.30

B. EXPERIMENTAL SETUP OF DAK-TL MEASUREMENTS

The DAK-TL was interconnected to VNA and PC as shown in Fig. 2. In this configuration, one port of the VNA was connected to the DAK-TL via a coaxial probe. The testing fixture was also linked with a PC via USB cable. Additionally, a LAN/Ethernet cable was used for connecting both the VNA and PC. Two probe beams, DAK 3.5-TL and 1.2E-TL, were used for measurements in different frequency ranges. The following settings were entered in the setup mode of the software, VISA address of the VNA, frequency segment for measurement, VNA output source power (O/P) = 0 dBm, VNA intermediate frequency (IF) Bandwidth = 100 Hz, probe beams that match the physical setup for the frequency of interest, the noise filter was activated to allow for smooth measurements, and the averaging reset of 3 VNA traces was selected to reduce the noise and the error of the reported result. Before starting the liquid measurements, DAK-TL was calibrated using the standard Open-Short-Load technique using distilled water at 20°C to achieve precise and reproducible measurements. A twenty-minute period was allowed for stabilizing the probe-connected coaxial cable then the calibration was performed and repeated multiple times until the measured and target data for the distilled water were greatly matched. Particularly, a precise volume of 10 mL was poured on a metallic petri-dish and placed on the automated sample platform that moved upwards for contacting the probe for measurement. The probe immersed inside the water sample a

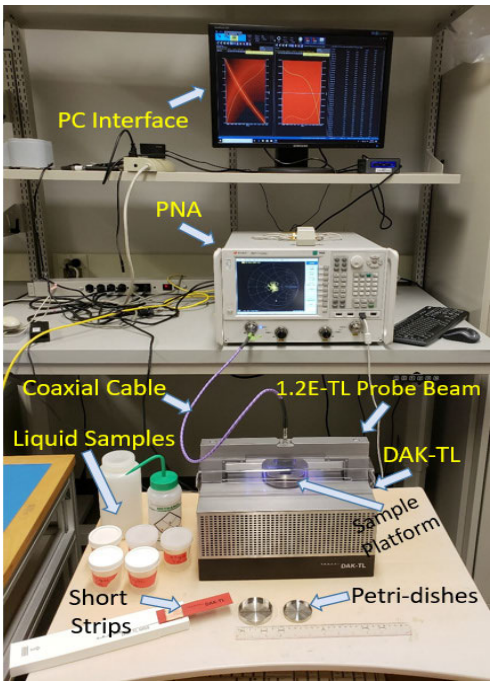

FIGURE 2. DAK-TL system setup for dielectric measurements of glucose solutions.

depth of 4 mm to have a good contact with no bubble underneath. In fact, these settings for the sample volume and probe depth were decided after studying the DAK-TL accuracy in measurements at different volumes of a tested liquid sample. That would also help to conclude the lowest volume of liquid that can be used for stable precise measurements.

C. DIELECTRIC MEASUREMENTS USING DAK-TL

The dielectric measurements were performed on four distinct frequency segments using two different probes, DAK 3.5-TL for 300 MHz–10 GHz (50 MHz resolution) and DAK1.2E-TL for measurements beyond 10 GHz at 200 MHz resolution. For measurements in each frequency portion, a 10 mL volume from each glucose sample was poured into the petri-dish and characterized by the system. The dielectric parameters extracted from the glucose measurements in (300 MHz–10 GHz), (6–30 GHz), and (30–50 GHz) bands have shown some variations that are not entirely linear as shown in Fig 3. As the frequency increases across the spectrum, the dependent dielectric permittivity and loss factor decreases and increases, respectively. However, the trend of both parameters with varying glucose levels is very hard to trace. Seemingly, the differentiation between various glucose concentrations of interest is not applicable in neither of these frequency bands. Likewise, the dielectric measurements of the 0.7–1.2 mg/ml glucose-water samples were investigated in the last mm-wave segment 50–67 GHz using the 10 mL volume. The extracted dielectric permittivity and loss tangent parameters demonstrate that the glucose concentrations of interest are better distinguishable in this higher frequency range as shown in Fig. 3. It is observed that

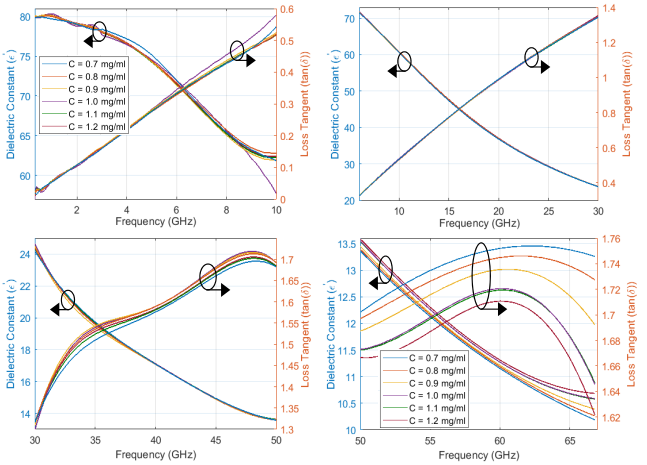

FIGURE 3. Dielectric measurements of glucose solutions at different frequency bands: 300 MHz - 10 GHz, 6 - 30 GHz, 30 - 50 GHz, and 50 - 67 GHz.

with an increased frequency in this interval, ϵ'_r of the glucose samples gradually decreases and the loss tangent increases in a nearly linear pattern before starting to decay exponentially after 60 GHz. Interestingly, with an increased glucose content in water, the dielectric permittivity slightly increases while the imaginary permittivity, conductivity, and loss tangent are all decreasing accordingly.

By comparing the collected dielectric measurements at lower frequency bands to those in the literature, we find that some researchers were able to achieve trend among glucose concentrations in such low frequencies but for higher concentrations than those considered in this study. For instance, the authors in [32] extracted the complex permittivity measurements for binary glucose-water solutions of concentrations in the range 1.0–5.0 mg/ml in the frequency band 1–8 GHz. Despite the non-linearity depicted in some variations of the collected data, a trend was observed at some frequencies posing a decrease in the dielectric constant and increase in the loss factor for an increased glucose level. The same trend could be observed when applying the Cole-Cole model parameters proposed in [33] for glucose-dependent EM properties of blood plasma to the glucose-water concentrations of 1–5 mg/ml. However, the changes depicted in the real and imaginary units of the permittivity are quite small in terms of ± 0.02 unit between various glucose concentrations. Interestingly, the Debye coefficients proposed in [26], [34] suggested a different varying trend in the dielectric parameters of such concentrations. Particularly, an increased dielectric constant and decreased loss factor over the frequency spectrum were recorded for increasing the glucose levels.

Following this study, the mm-wave frequency range has shown to be promising for glucose sensing where higher sensitivity to the dielectric constant and loss tangents of glucose samples can be acquired as a result of the stronger interaction between the glucose molecules and EM waves in this spectrum. Therefore, the proposed WGM sensor is decided to operate in this mm-wave band. For this purpose,

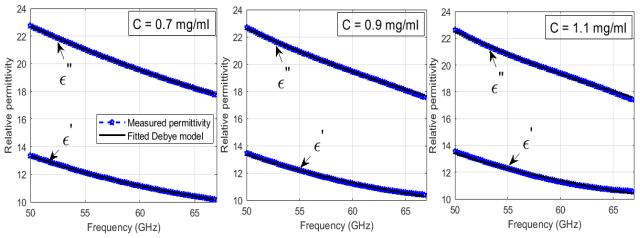

FIGURE 4. Dielectric measurements of the relative permittivity fitted to proposed Debye model for C = 0.7, 0.9, and 1.1 mg/ml.

the measured dielectric parameters of the glucose samples are fitted to a single-pole Debye model to be used for analyzing the sensitivity performance of the designed WGM sensor when loaded with the glucose concentrations of interest via integrating their dielectric values in the numerical simulator at a certain frequency. More details about these steps will be explained in the next sections of this paper.

D. FITTING TO A SINGLE-POLE DEBYE MODEL

In this subsection, a dispersive concentration-independent model is formulated by fitting the collected dielectric measurements in the mm-wave frequency range (50–67 GHz) for the relative permittivity of the tested glucose solutions using the first order (single-pole) Debye relaxation model. In particular, the real ϵ_r' and imaginary ϵ_r'' parts of the measured permittivity for each glucose sample of a definite concentration were fitted to the theoretical Debye model defined by (4) and (5), respectively, where ϵ_{stat} is the static permittivity (at zero frequency), ϵ_∞ is the infinity permittivity, τ is the relaxation time, and ω is the angular frequency

$$\epsilon_r'(w) = \epsilon_\infty + \left(\frac{\epsilon_{stat} - \epsilon_\infty}{1 + (\omega\tau)^2}\right) \tag{4}$$

$$\epsilon_r''(w) = -\frac{\omega\tau(\epsilon_\infty - \epsilon_{stat})}{1 + (\omega\tau)^2} \tag{5}$$

The parameters proposed in [26] were used as initial values for ϵ_{stat}, ϵ_∞, and τ for the fitted curves. An optimization routine is coded to minimize the standard squared deviation (SSD) error between the measured and modelled data as given in (6) using the Generalized Reduced Gradient (GRG) algorithm that was run multiple time to converge the Debye curves to the collected measurements

$$\min_{\epsilon_\infty, \epsilon_s, \tau} SSD = \sum (measured - model)^2 \tag{6}$$

A better fit to the measured data of the dielectric constant and loss factor for each glucose concentration was achieved by extracting one group of Debye coefficients for each glucose sample. Specifically, the extracted coefficients are functionally independent of the glucose concentration ξ in the tested glucose-water solution. Figure. 4 shows these fitted curves for the glucose samples of $C = 0.7$, 0.9, and *1.1 mg/ml*. Table 2 presents all the extracted coefficients for modelling the complex permittivity of each glucose concentration in the frequency range 50–67 GHz, the minimum squared deviation error (SSD) obtained for each fitting, and the dielectric properties highlighted at $f = 60\ GHz$ for general illustration of the varying trend.

TABLE 2. Proposed Debye coefficients and dielectric properties at 60 GHz for each glucose concentration.

Glucose samples (mg/ml)	ϵ_∞	ϵ_s	τ (ps)	SSD	ϵ_r' ($f = 60$ GHz)	$tan\delta$ ($f = 60$ GHz)
0.7	5.67	80.650	9.42	0.014	11.15	1.75
0.8	5.76	81.028	9.49	0.029	11.19	1.74
0.9	5.92	81.950	9.65	0.119	11.23	1.73
1.0	6.13	82.950	9.82	0.322	11.27	1.72
1.1	6.15	83.208	9.85	0.346	11.31	1.71
1.2	6.27	83.790	9.95	0.485	11.35	1.70

IV. THE PROPOSED GLUCOSE SENSING APPROACH

We propose a simple integrated WGM sensor operating in the mm-wave range 50–70 GHz to be used as a sensing platform for tracking the variations in glucose concentration levels in blood mimicking samples. This sensor is composed of dielectric disc resonator (DDR) coupled to a dielectric image waveguide (DIG) that is basically employed for exciting the WGM modes inside the DDR by linking the residual evanescent tail of the guided field. The induced WGM waves propagate circularly around the centre of the DDR towards its cylindrical boundaries in rotations of integer multiple of 2π phase shifts and with repeated total reflections from the DDR edges. The resulting resonant modes triggered inside the DDR are either WGE_{nml} of transverse electric-field (i.e. quasi-TE) or WGH_{nml} of an axial electric-field (i.e. quasi-TM) modes, where the integer subscripts *n, m,* and *l* represent the order of the azimuthal, radial, and axial dependencies, respectively. For our proposed glucose sensor, we are more interested in WGE_{n00} and WGH_{n00} modes that are advantageous for effective sensing by the highly concentrated EM energy confined near the frontiers of the DDR.

Following the last point, the sensing method on such WGM resonators is based on the resonant perturbation of the excited WGM modes (i.e. perturbing their evanescent field distribution), and therefore modifying one or all the intrinsic resonance attributes, resonance frequency and/or *Q*-factor, in the presence of the SUT, which are the glucose samples in our case. The tested glucose sample is placed inside a cylindrical container on top of the DDR surface where the rims are highly intensified with the WGM electric-fields, thereby acquiring greater interactions with the tested glucose sample at a given mm-wave resonant frequency. Consequently, the resulting changes in the WGM resonance characteristics are considered as a unique signature of the dielectric properties of the tested glucose sample that can be identified by carefully calibrating the sensing parameters for this WGM sensing structure. More insights into these sensing parameters are illustrated by studying the mathematical model of the WGM resonators in the next subsection.

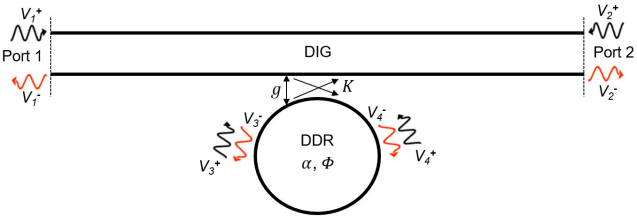

FIGURE 5. Approximated four-coupler model of the unloaded WGM sensor.

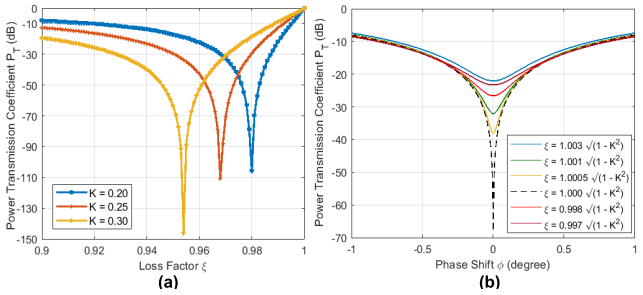

FIGURE 6. Transmission coefficient variations at resonance as function of (a) loss factor of the DDR for different coupling coefficients, (b) phase delay per rotation inside the DDR for different loss factors.

A. MATHEMATICAL (COUPLING) MODEL OF REACTION-MODE WGM RESONATORS

The WGM sensor scheme of the dielectric disc resonator (DDR) coupled to the dielectric image waveguide (DIG) can be approximated with a four-port coupler [35] as depicted in Fig. 5 where the power is transmitted from port 1 to port 2 (or vice versa). Ports 3 and 4 are virtual ports around the DDR to illustrate the coupled-wave behavior that is travelling forward and backward around the DDR (i.e. like a transmission line) as given by $V_3^- = e^{-\gamma} V_4^+$ and $V_4^- = e^{-\gamma} V_3^+$, where γ is the complex propagation coefficient. Under resonance condition, the WGM sensor exhibits a band-stop filter characteristics where the DDR absorbs almost all the fed power and leaves nothing to appear at the receiving port.

The two-ports transmission coefficient S_{21} (insertion loss) of this WGM resonator can be derived from the scattering matrix of the four-port coupler while substituting the forward and backward relations for the waves presenting at ports 3 and 4, as follows [35]

$$S_{21} = \frac{\sqrt{1-K^2} - e^{-(\alpha+j\Phi)}}{1-\sqrt{1-K^2}e^{-(\alpha+j\Phi)}} \tag{7}$$

where α is the resonator attenuation coefficient, Φ is its phase delay parameter that equals $2n\pi$ at the resonance condition, and K is the coupling coefficient between the waveguide and the resonator. Therefore, the DIG-to-DDR power transmission coefficient and phase will be

$$P_T = |S_{21}|^2 = \frac{\left(1-K^2\right) + \xi^2 - 2\xi\sqrt{1-K^2}cos\Phi}{1+\left(1-K^2\right)\xi^2 - 2\xi\sqrt{1-K^2}cos\Phi} \tag{8}$$

$$\Theta_T = \angle S_{21} = \tan^{-1}\frac{\xi K^2 \sin\Phi}{\sqrt{1-K^2}\left(1+\xi^2\right) - \xi\left(2-K^2\right)cos\Phi} \tag{9}$$

The loaded quality-factor (Q_L) of the WGM sensor is also dependent on the attenuation and the coupling coefficient as given by [36]

$$Q_L = \frac{n\pi}{\xi\sqrt{1-K^2}}\sqrt{\frac{1+\left(1-K^2\right)\xi^2}{2}} \tag{10}$$

where $\xi = e^{-\alpha}$ is the loss factor of the DDR representing the normalized amplitude of the WGM travelling-wave after one circular rotation around the resonator. ξ ranges from a minimum value of 0 (quite lossy) up to the maximum of 1 (a lossless DDR with zero attenuation). The coupling coefficient K has a similar range from 0 to 1, where $K = 0$ represents the no coupling state with zero power transferred to the DDR and $K = 1$ indicates the critical coupling state at which all the fed power from the input port is coupled to the DDR leaving nothing to appear at the receiving port ($S_{21} = 0$) as long as the resonance is occurring. By substituting the resonance conditions of $S_{21} = 0$ and $\Phi = 2n\pi$ in (8) we derive the relation that defines the critical coupling state where the K and ξ are inversely related.

$$\xi = \sqrt{1-K^2} \tag{11}$$

This critical coupling state is an exceptional feature for the WGM travelling-wave sensors. It can be exploited to acquire an extremely high sensitivity in the transmission response when the sensor is perturbed at any of its parameters Φ, ξ, and K. This is demonstrated in Fig. 6(a) which shows the critical coupling resonances in the transmission response for different values of the coupling coefficients $K = 0.2, 0.25,$ *and* 0.3 that meet the criteria in (11) when $\Phi = 2n\pi$. Figure. 6(b) depicts the transmission coefficient response as a function of the phase shift per rotation inside the DDR for a specific coupling coefficient value at $K = 0.2$ and with different values for the loss factor ξ. It is clearly observed the dependency of the transmission resonant peak on the ξ parameter of the DDR. In particular, for a relatively large value of ξ than the equality in (11), the resonant peak is about -22dB then it starts dipping down gradually with small perturbation in ξ. The critical coupling resonance of the deepest amplitude occurs when this ratio equals unity as shown with the dashed black curve. When ξ is getting smaller beyond this equality, the resonant peak starts decreasing again to unlock the critical coupling state.

B. COUPLING COEFFICIENT AND LOSS FACTOR DEPENDENCIES

In this subsection we discuss the factors that affect the coupling coefficient K and the loss factor ξ for the WGM sensor. First, the coupling coefficient K is considerably dependent upon the spacing distance g between the DIG and the DDR. This is illustrated very clearly in Fig. 7 that depicts the simulated transmission responses (insertion loss) at

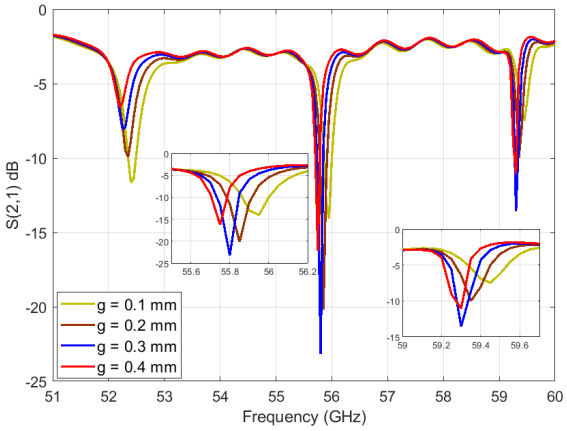

FIGURE 7. Simulated transmission coefficients for the unloaded DDR at different gap distances.

different spacing for the WGH_{600}, WGH_{700}, and WGH_{800} excited modes. The transmission resonances are shifted in frequency and varied in Q-factor with g changing between 0.1 to 0.4 mm. The plot also implies a near critical coupling state for the WGH_{700} and WGH_{800} modes when the spacing is set around $g = 0.3mm$, this would clearly emphasize that stronger coupling is not necessarily achievable by setting the DDR very close to the driving DIG. In fact, for a given amount of loss within the DDR, the strongest coupling occurs only at a specific distance between the DDR and the DIG, and if the resonator loss changes then the critical coupling will be defined for another gap distance. This statement suggests that the coupling coefficient K is also a function of the amount of loss in the DDR as well as the loaded sample. This interesting phenomenon will be shown later when the lossy glucose samples are loaded on top of the DDR resulting into a new set of critical coupling conditions that differ from the one shown in Fig. 7 for the unloaded DDR for all the supported WGH modes. The second important parameter for the WGM sensor is the loss factor ξ of the utilized DDR represented by the loss tangent $tan\delta$ property of its fabricated material. Generally, higher losses within the DDR will affect the transmission response by decreasing the transmitted power to the receiving port. It may also decrease the resonance depth of the WGM mode, however, the strongest WGM coupling could occur at a specific loss tangent for the DDR that is not necessarily be the lowest in value.

The aforementioned features will be advantageous for sensing the glucose level when the tested sample is integrated on top of the DDR. The resonance characteristics of the combined sensor would become very sensitive to any small perturbation close to its boundary region making the sensor capable of differentiating various glucose concentrations with subtle differences in EM properties.

V. WGM SENSITIVITY ANALYSIS FOR GLUCOSE DIELECTRIC PROPERTIES

In what follows, we study the theoretical sensitivity of the WGM sensor to the variations in the dielectric properties (i.e. complex permittivity) of the tested samples of glucose-loaded watery solutions that are placed inside a cylindrical container on top of the DDR. The tested samples have complex relative permittivity of $\epsilon_{rg} = \epsilon'_{rg} - j\epsilon''_{rg}$ where both the real and imaginary parts have large values that vary based on the amount of glucose dissolved in the sample as discussed earlier. The DDR underneath the glucose sample also has a complex relative permittivity of $\epsilon_{rDR} = \epsilon'_{rDR} - j\epsilon''_{rDR}$ with small real and imaginary parts that are fixed in value. The integrated structure of the DDR and the tested glucose sample are placed at a specific distance g from the exciting DIG. The interaction between the loaded glucose sample and the WGM evanescent field induced by the DDR is reflected in the measured transmission coefficient and phase of the entire structure as given by (8) and (9).

To account for the two varying properties of the tested glucose samples, the sensitivity of the sensing parameters P_T and Θ_T are defined for the real and imaginary parts of the glucose sample permittivity whose effects appear more dominantly in the phase delay per rotation inside the DDR and its loss factor, respectively. Therefore, the sensitivity expressions can be written as follows using the chain rule for partial derivatives.

$$S_{P_T}^{real} = \frac{\partial P_T}{\partial \epsilon'_{rg}} = \frac{\partial P_T}{\partial \Phi}\frac{\partial \Phi}{\partial \epsilon'_{rg}} \tag{12}$$

$$S_{P_T}^{imag} = \frac{\partial P_T}{\partial \epsilon''_{rg}} = \frac{\partial P_T}{\partial \xi}\frac{\partial \xi}{\partial \epsilon''_{rg}} \tag{13}$$

$$S_{\Theta_T}^{real} = \frac{\partial \Theta_T}{\partial \epsilon'_{rg}} = \frac{\partial \Theta_T}{\partial \Phi}\frac{\partial \Phi}{\partial \epsilon'_{rg}} \tag{14}$$

$$S_{\Theta_T}^{imag} = \frac{\partial \Theta_T}{\partial \epsilon''_{rg}} = \frac{\partial \Theta_T}{\partial \xi}\frac{\partial \xi}{\partial \epsilon''_{rg}} \tag{15}$$

The terms $\frac{\partial P_T}{\partial \Phi}$, $\frac{\partial P_T}{\partial \xi}$, $\frac{\partial \Theta_T}{\partial \Phi}$, and $\frac{\partial \Theta_T}{\partial \xi}$ are derived by differentiating (8) and (9) with respect to the corresponding parameters of $\Phi$and ξ. When the critical coupling condition for the integrated sensor is satisfied, these terms will be at their maximum values. This is very clearly illustrated in Fig. 6(a) and 6(b) that show the variation in P_T as function of the loss factor of the DDR and the phase shift per rotation, respectively. The variations in $\frac{\partial \Theta_T}{\partial \Phi}$, and $\frac{\partial \Theta_T}{\partial \xi}$ can be depicted using similar plots.

The term $\frac{\partial \Phi}{\partial \epsilon'_{rg}}$ in (12) and (14) can be calculated indirectly by relating the phase delay parameter Φ to the WGM resonant frequency f_r as given in (16) assuming that the axial propagation constant k_z is very small compared to the quantity $\sqrt{\epsilon}'_{rDR}k_o$, where ϵ'_{rDR} is the dielectric constant of the DDR and k_o is the free-space wave-number [37]

$$\frac{\partial \Phi}{\partial \epsilon'_{rg}} = 4\pi^2 R\frac{\sqrt{\epsilon}'_{rDR}}{C}\frac{\partial f_r}{\partial \epsilon'_{rg}} \tag{16}$$

where R is the radius of the DDR, C is the speed of light in vacuum, and $\frac{\partial f_r}{\partial \epsilon'_{rg}}$ is the sensitivity of the resonant frequency with respect to the real permittivity of the glucose sample. The latter can be determined via numerical analysis for the

shifts in f_r for a given WGH_{n00} mode due to the change in the sample dielectric constant.

Similarly, the term $\frac{\partial \xi}{\partial \epsilon''_{rg}}$ in (13) and (15) is determined by formulating the loss factor of the DDR as a function of the unloaded Q-factor of the sensor structure asymptotically as given in (17), in the near resonance [36]. By differentiating this quantity with respect to the sample imaginary permittivity we obtain the relation in (18).

$$\xi = e^{\left(-\pi R k_o \sqrt{\epsilon'_{rDR}} Q_U^{-1}\right)} \tag{17}$$

$$\frac{\partial \xi}{\partial \epsilon''_{rg}} = -\xi \ln(\xi) Q_U^{-1} \frac{\partial Q_U}{\partial \epsilon''_{rg}} \tag{18}$$

where $\frac{\partial Q_U}{\partial \epsilon''_{rg}}$ is a figure of merit that defines the sensitivity of the Q-factor of the integrated sensor with respect to the glucose imaginary permittivity. It can be calculated as in (20) by the partial derivative of (19) [38]

$$\frac{1}{Q_U} = E_{DR} \tan \delta_{DR} + E_g tan\delta_g + \frac{1}{Q_{con}} + \frac{1}{Q_{rad}} \tag{19}$$

$$\frac{\partial \xi}{\partial \epsilon''_{rg}} = \xi_o \ln(\xi_o) Q_U \frac{\partial \epsilon_g}{\partial \epsilon'_{rg}} \tag{20}$$

By substituting (16) and (20) in the sensitivity expressions (12)–(15), we can clearly see that the sensitivity of a given WGM resonant mode with respect to the glucose real permittivity (dielectric constant) is determined by the resultant shifts in its resonant frequency. While the WGM sensitivity to changes in the imaginary permittivity (loss property) can be obtained by tracking the changes in the corresponding Q-factor. This sensitivity is also directly proportional to the Q-factor of the DDR; which means that higher sensitivity can be acquired by having DDR of larger Q-factor.

VI. THE PROPOSED MM-WAVE SENSOR DESIGN, SIMULATIONS AND MEASUREMENTS

A. DESIGN AND SPECIFICATIONS

The WGM sensor structure consists of a Dielectric Image Guide (DIG) coupled to a dielectric disc resonator (DDR) with both installed on top of a planar metallic support structure. The DIG with the low-loss, easy-to-manufacture, and wide-band performance characteristics in the mm-wave band is designed in two different layouts, straight and curved. Both layouts of the DIG are linearly tapered at both ends to reduce the loss caused by the possible scattering and reflection at the discontinuities, and to strengthen its coupling to the rectangular metallic waveguide. Both DIG and DDR are integrated inside a rectangular metallic waveguide and excited via metallic wave ports/adaptors (WR-15) to support the dominant mode (E_z^{11}) operation in the mm-wave frequency band of interest, resulted into operating the DDR in WGH modes. However, exciting the structure by means of a metallic waveguide could possibly excite the E_x^{11} mode inside the DIG, therefore it should not be triggered. The DIG is used for exciting the WGM modes with travelling-wave resonances inside the DDR by linking the evanescent tail of the guided field that is mostly confined inside the dielectric waveguide region to the neighboring dielectric resonator. The width parameter of the DIG is crucial in controlling the spread of the evanescent tail exploited for coupling the power into the DDR. In particular, an evanescent field with longer tail would be realized by fabricating the DIG with smaller width, and therefore making the DIG-to-DDR coupling less sensitive to their separating gap g. Following that, the exciting DIG was fabricated using Alumina of dielectric constant $\epsilon'_r = 9.2$ and loss tangent $tan\delta = 0.0005$, for its fairly low-loss, easy-to-fabricate, and low-cost. It has a cross section of 1×0.8 mm^2 (width $W = 0.8mm$, height $H = 1mm$) and a total length of 50 mm with linear tapers at both ends to reduce the insertion and return losses.

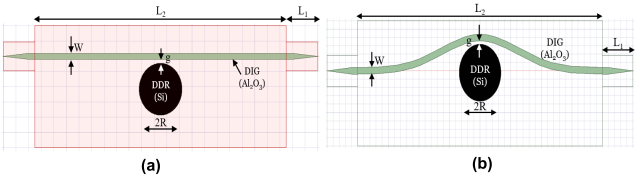

FIGURE 8. The design geometries of the proposed sensor structures with (a) straight DIG and (b) curved DIG, before loading glucose samples (top view).

The DDR was fabricated from a low-loss Silicon material of dielectric constant $\epsilon'_r = 11.6$ and loss tangent $tan\delta = 0.001$ using the Deep Reactive Ione Etching (DRIE). It is pivotal to consider the WGM mode number as a deigned parameter when designing the DDR for sensing applications. Low-order modes ($n < 5$) for example are radiating with low Q-factor while the relatively higher-order modes ($n > 10$) require a larger size of DDR for operating in the same desired range of frequency. Additionally, such higher-order modes are very confined around the DDR boundary with a very small evanescent field tail that is not adequate to sense any external perturbations outside of DDR. With that being considered, the DDR is designed accordingly in a disk shape with axial height $h = 0.5mm$ and radius $R = 3.42mm$ such that the minimum mode number of WGM is larger than 5 over the desired range of frequency 50–70 GHz to enhance the mode confinement and minimize the radiation. All these design specifications and geometries were set after simulating the sensing structure using the 3D EM solver of High Frequency Structure Simulator (ANSYS HFSS) as will be explained in the next subsection.

B. NUMERICAL SIMULATIONS OF THE WGM SENSORS

The proposed design of the sensor structure shown in Fig. 8(a) with a straight DIG was simulated with the parameters shown in Table 3, before loading any glucose samples, using ANSYS HFSS. The gap between the DIG and DDR was set initially to $g = 0.5\ mm$. The driven solution of the simulation model was set with the appropriate parameters of solution frequency, maximum number of passes, delta S for allowable variation between consecutive meshes, and minimum converged passes. The port and meshing sizes were chosen to achieve the

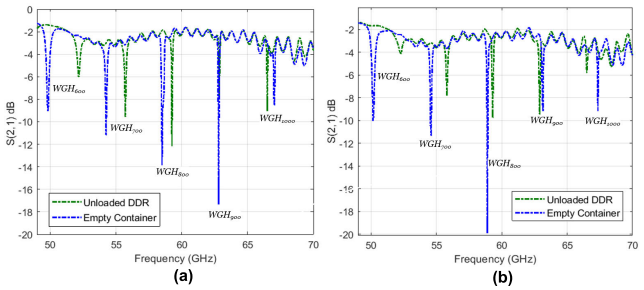

FIGURE 9. Simulated transmission coefficients on 50–70 GHz mm-wave band for different DDR states and the corresponding WGM modes (a) straight DIG and (b) curved DIG.

TABLE 3. Design parameters of the sensor structures shown in Fig. 8.

Parameter	W	H	L_1	L_2	R	h	R_c	Θ_c
(mm)	0.8	1.0	5.0	40	3.42	0.5	4.0	45°

convergence criteria accordingly. In another layout, the DIG was simulated with a curvature ($R_c = 4$mm, $\theta_c = 45°$) in the area around the DDR to realize a more compact packaged system as shown in Fig. 8(b). It has a similar cross section of 1×0.8 mm^2 and a total length of 50 mm with linear tapers at both ends. The taper parts have a length of $L_2 = 5mm$ each. The simulated S_{21} transmission curves as function of the frequency for both layouts straight and curved, are plotted in Fig. 9(a) and 9(b), respectively, in the entire mm-wave band 50–70 GHz when the DDR is unloaded (dashed green color). Five distinct WGH resonance modes are observed in this band as labelled accordingly in each plot, WGH_{600}, WGH_{700}, WGH_{800}, WGH_{900}, and WGH_{1000}. The few ripples shown are due to the imperfect coupling at $g = 0.5$ mm.

A plexiglass container of dielectric constant $\epsilon_r' = 3.4$ and loss tangent $tan\delta = 0.001$ was integrated on top of the DDR to hold the liquid samples of various glucose concentrations as shown in the final designs in Fig. 10.

The parametric sweep function in HFSS was used to optimize the sensitivity performance of the integrated sensor when loaded with glucose samples inside the plexiglass container. First, it was desired to achieve strong coupling between the DDR and glucose sample inside the container, therefore it was necessary to design the sample container properly to acquire the highest sensitivity at each WGM mode. Specifically, the bottom thickness t_2 of the container was observed to considerably affect the coupling between the DDR and the glucose sample inside the container when swept from 0 mm to 3 mm. The thickness of $t_2 = 1.5mm$ was resulted into better coupling as illustrated in Fig. 11(a) and 11(b), respectively, thereby it was used to design the integrated sample container. While the thickness for the side-wall t_1 has no significant effect. Based on these observations, the container was designed with height $h_c = 7mm$, side and bottom thickness $t_1 = 0.1mm$ and $t_2 = 1.5$ mm, respectively. Loading the clear empty container on top of the DDR would result into small shifts in the resonant frequencies for each

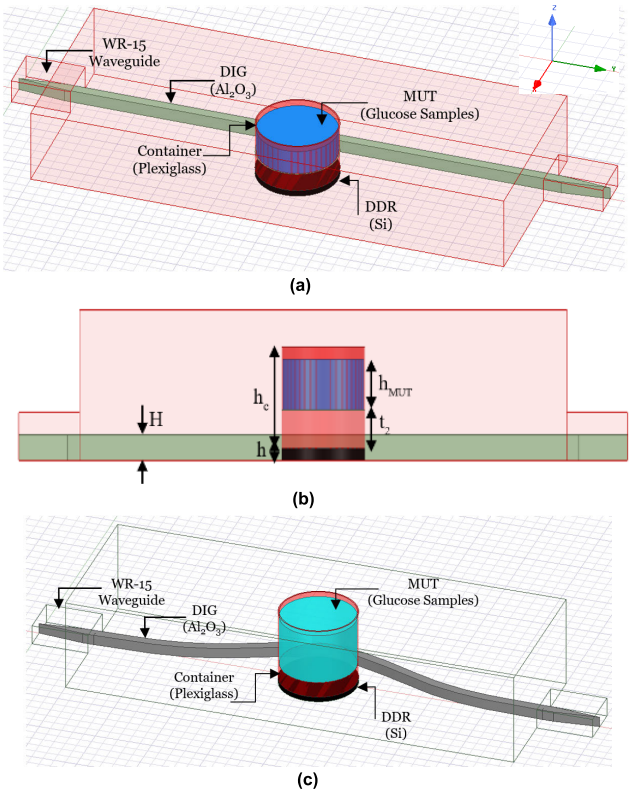

FIGURE 10. The final integration and geometrical parameters of the proposed WGM sensors with straight DIG (a) 3D view, (b) side view, and curved DIG (c) 3D view.

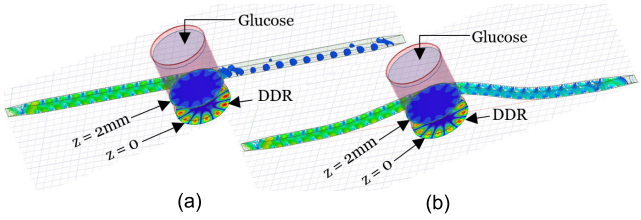

FIGURE 11. The electric-field distribution inside the dielectric waveguide, bottom surface of the DDR (z = 0), and inside the glucose sample (z = 2 mm) for (a) straight DIG and (b) curved DIG.

WGH mode as depicted in Fig. 9(a) and 9(b) for the straight and curved layouts, respectively. It is observed that the shift exhibited at each WGH mode is different from other modes.

Second, we also aimed at creating a critical coupling between the loaded dielectric resonator and the dielectric waveguide at the different supported WGH modes in order to obtain the largest Q-factor with steepest resonant dips for effective sensing. Such conditions were determined by sweeping the gap parameter g from 0.1mm to 0.8mm in steps of 0.1mm when the structure was loaded with different glucose samples at each WGH resonance frequency. Interestingly, for a given WGH mode the resonator would have the same critical coupling gap when loaded with the different glucose samples. This is demonstrated in Fig. 12 that shows a critical coupling resonance at $f = 54.1$ GHz for the WGH_{700} mode when the spacing was set to $g = 0.5$ mm

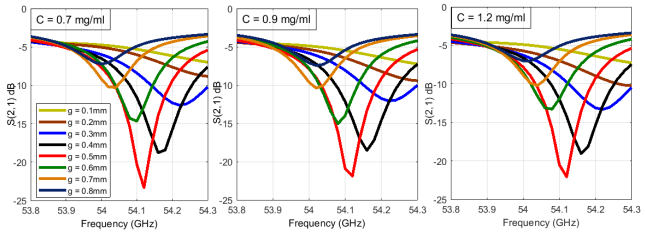

FIGURE 12. Transmission curves for WGH_{700} mode at different gaps between the DIG and DDR. The DDR has the same critical coupling gap when loaded with glucose samples of 0.7, 0.9, and 1.1 mg/ml.

TABLE 4. Critical coupling gap and sensitivity for each WGH mode for the straight and curved WGM sensors.

	Straight DIG		Curved DIG	
WGH Mode	Critical Coupling Gap *g (mm)*	Sensitivity (dB/[mg/ml])	Critical Coupling Gap *g (mm)*	Sensitivity (dB/[mg/ml])
WGH_{600}	0.50	3.10	0.42	7.70
WGH_{700}	0.50	2.50	0.45	2.50
WGH_{800}	0.30	0.40	0.45	1.04
WGH_{900}	0.50	0.30	0.40	0.30

between the waveguide and the loaded resonator with 0.7, 0.9, and 1.1 *mg/ml* glucose samples. The variation in the amount of loss in these glucose concentrations is very small as shown earlier, therefore the resultant effective loss for the integrated resonator (DDR + glucose-varying sample) will hold the same critical coupling gap at various concentrations. However, this critical coupling condition is varying from one WGH mode to another as shown in Table 4.

To determine the critical coupling gap for each individual WGH mode, separate simulations were performed for the loaded DDR at the appropriate frequencies corresponding to each WGH mode while varying the gap parameter g. Table 4 presents the critical coupling gap for each WGH mode and for both sensor layouts, straight and curved. Finally, we studied the sensitivity behavior of both WGM sensors under the critical coupling condition for each supported WGH mode for the glucose level variations in the loaded samples 0.7, 0.8, 0.9, 1.0, 1.1, and 1.2 *mg/ml*. Different glucose concentrations were simulated by integrating their dispersive EM properties, dielectric constant and loss tangent, in the HFSS simulator using the single-pole Debye model with the independent coefficients in Table 2 as extracted from the DAK-TL mm-wave measurements.

In these simulations, it is interesting to note that the first lower modes WGH_{600} and WGH_{700} exhibit higher sensitivity for changes in glucose levels compared to the higher order modes WGH_{800}, WGH_{900},and WGH_{1000} in the mm-wave range. For example, for the straight-DIG sensor operating at WGH_{600} and WGH_{700}, the $|S_{21}|$ varies by 0.31 dB and 0.25 dB, respectively, for 0.1 mg/ml increase in glucose concentration (e.g. from 0.7 to 0.8 mg/ml), while this variation in $|S_{21}|$ is shown to be around 0.04 dB and 0.03 dB in the

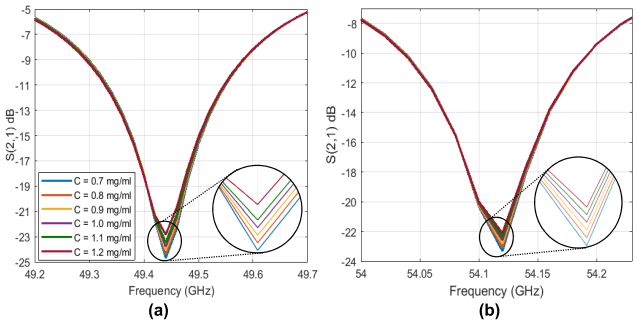

FIGURE 13. Simulated transmission coefficients for different glucose concentrations loaded on the straight WGM sensor at the WGH_{600} and WGH_{700} resonant modes.

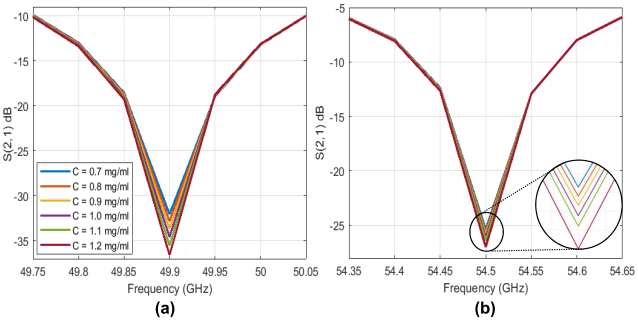

FIGURE 14. Simulated transmission coefficients for different glucose concentrations loaded on the curved WGM sensor at the WGH_{600} and WGH_{700} resonant modes.

higher modes WGH_{800} and WGH_{900}, respectively, for a similar change in glucose level. Similar phenomena were recorded for testing the glucose samples using the curved-DIG sensor. However, its sensitivity performance to variations in glucose levels is shown to be higher at the two lower-order WGH modes compared to that of the straight-DIG as demonstrated by the sensitivity simulated for both using $\Delta S_{21}/\Delta C$ in dB/[mg/ml] as listed in Table 4 for each WGH mode. Figure 13(a) and 13(b) show the transmission responses for the different glucose samples at WGH_{600} and WGH_{700}, respectively, when tested using the straight-DIG sensor. Figure 14(a) and 14(b) plot these transmission responses at WGH_{600} and WGH_{700}, respectively, when the curved-DIG sensor is used. The amplitude resolution of the transmission coefficient for the glucose level changes at both modes WGH_{600} and WGH_{700} is plotted in Fig. 15(a) and 15(b), for the two WGM sensors.

The phase of $S_{21}$was also observed to be sensitive to glucose level variations in the lower-order WGH modes. Figure. 16(a) and 16(b) depict the phase responses to glucose level changes when the WGH_{600} mode was excited inside the sample using the straight-DIG and curved-DIG, respectively. For the straight-DIG case for example, the phase changes by 1.2° and 0.7° on average at $f = 49.4\ GHz$ and $f = 49.48\ GHz$, respectively, for any 0.1 mg/ml change in glucose. However, the phase response of the curved-DIG sensor varies by 4° at $f = 49.9\ GHz$ for a similar change in glucose level.

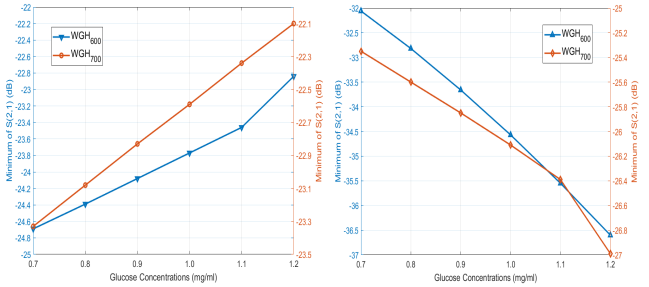

FIGURE 15. The resolution of the resonant amplitude at WGH_{600} and WGH_{700} for the glucose level changes for (a) straight and (b) curved sensor.

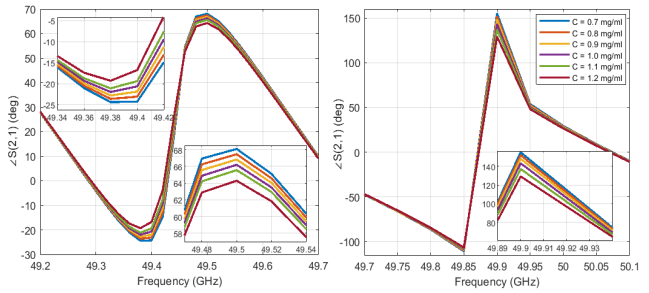

FIGURE 16. Simulated transmission phases for different glucose concentrations loaded on the (a) straight and (b) curved WGM sensor at the WGH_{600} resonant mode.

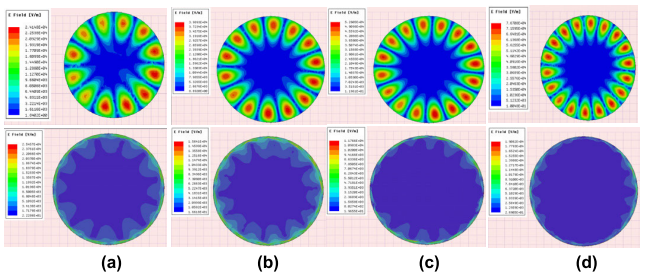

FIGURE 17. Electric-field distribution at the bottom surface of the DDR z = 0 (top) and inside the glucose solution at z = 2mm (bottom) for different WGM resonances (a) WGH_{600} (b) WGH_{700} (c) WGH_{800} (d) WGH_{900}.

This tendency in sensitivity could be interpreted by the nature of the interaction between the coupled WGM field and the glucose sample inside the container at each WGH mode as demonstrated in Fig. 17 that shows the electric-field distribution induced at each WGH resonance mode inside the DDR at the bottom surface z=0 (first row) and inside the glucose at the sample floor z=2mm (second row). Particularly, it is clearly seen that the lossy glucose molecules have greater interactions with the coupled evanescent fields at the lower-order modes WGH_{600} and WGH_{700} (Fig. 17(a) and 17(b)) compared to the higher-order modes WGH_{800} and WGH_{900} (Fig. 17(c) and 17(d)) that generate very small evanescent tails not adequate to sense the small external perturbations of the glucose dielectric constant and loss outside the DDR.

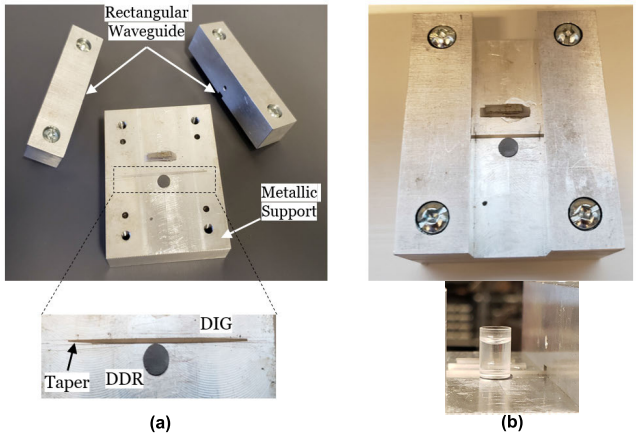

FIGURE 18. Fabricated prototype of the straight WGM sensor (a) installing the DDR and DIG on top of a metallic support (b) integrating all the parts with the rectangular metallic waveguide (top view). Glucose sample inside a container on top of a DDR.

C. EXPERIMENT SETUP AND MEASUREMENTS OF WGM GLUCOSE SENSING

The fabricated DIG and DDR were combined and installed on top of a metallic support structure as shown in Fig. 18(a). The gap distance between the DDR and DIG was reasonably set to around *0.5 mm* to maximize the sensitivity at different WGM resonances. Small drops of a low-loss epoxy glue were used to stabilize the position of the DIG and DDR over the metallic base. Fixing the DIG from both sides with a glue has a negligible increment in the loss and should not affect the field distribution of the desired mode inside the DIG which is nearly confined in the centre of the structure. The DDR should be installed very carefully using an epoxy drop in the middle as the field coupled to the resonator is very sensitive to any small perturbations. The final sensor structure after integrating with the rectangular waveguides is shown in Fig. 18(b). The DDR loaded with the glucose-filled container is also shown.

Two rectangular metallic waveguide adaptors (WR-15) were used to couple the power in and out of the DIG as shown in the complete experimental setup captured in Fig. 19 that consists of a Vector Network Analyzer (PNA-X) connected to a screen, two harmonic mixers/extenders at V-band connected to the integrated WGM sensor device via the WR-15 ports. The preliminary prototype was tested when unloaded over the V-band to verify the overall functionality that exhibits five WGM resonances (WGH_{600}, WGH_{700}, WGH_{800}, WGH_{900}, and WGH_{1000}) as depicted in Fig. 19 at frequencies f = 51, 55, 59.06, 63.2, and 67.42 GHz, respectively (green solid curves).

To probe into the fabricated sensor capability and sensitivity for detecting the glucose concentrations, we loaded the Silicon-made DDR with an empty container and used some of the prepared glucose-water samples for testing its functionality. The container was fabricated from a plexiglass material with the following dimensions (t_1 = 1mm, t_2 = 1.5mm,

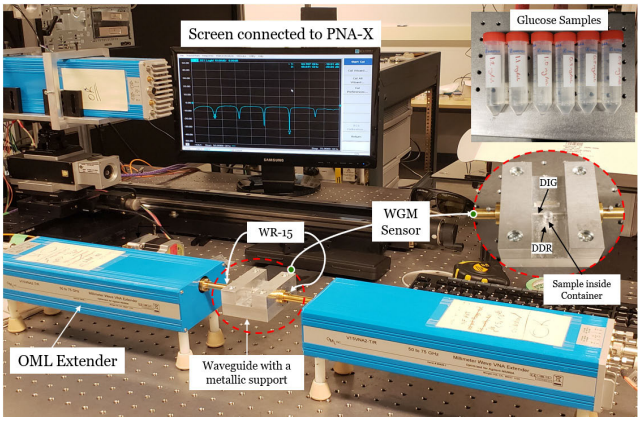

FIGURE 19. The experimental setup for WGM measurements.

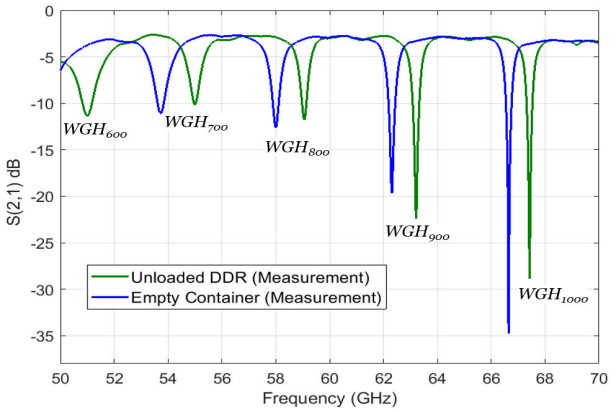

FIGURE 20. Measured transmission response of the WGM sensor in the mm-wave range when unloaded and loaded with empty container.

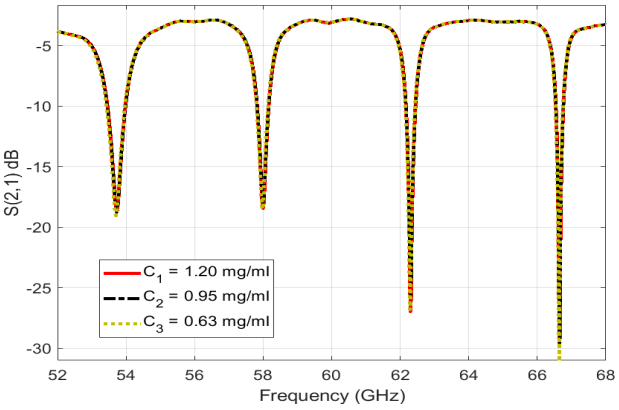

FIGURE 21. Measured WGM resonances for various tested concentrations.

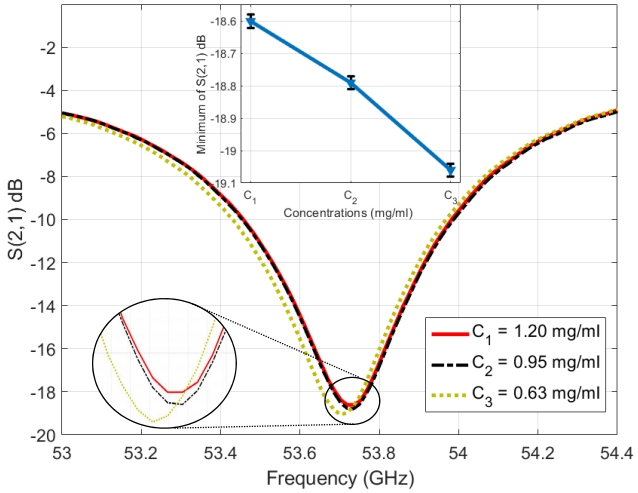

FIGURE 22. Resonant amplitude variations at different tested glucose concentrations when WGH_{700} is excited.

$h_c = 10mm$) that can hold a total volume of $V_c = 0.37mL$ of liquid inside. Loading the empty container on top of the DDR would result into shifting all the WGH resonances towards lower frequencies as depicted in Fig. 20 (blue solid curves).

After that the glucose samples were loaded at specific volumes inside the container using a micropipette device. To elaborate this proof-of-concept test, the combined DDR-container resonator was loaded with three different glucose concentrations (C_1, C_2, *and* C_3). First, we added one drop of volume ($V_1 \approx 0.1\ mL$) of glucose-water solution of concentration $C_1 = 1.2\ mg/ml$ and noticed the change in the Q-factors for all the WGH modes including WGH_{700} as shown in Fig. 21 (red solid curve). To test the sensor for another concentration it would be more convenient to add a drop of another concentration to avoid any difficulties in removing the first added drop of concentration C_1. Therefore, the second tested concentration C_2 was formed by adding a drop of similar volume ($V_2 \approx 0.1\ mL$) of 0.7 mg/ml to that of 1.2 mg/ml inside the container resulting into a new diluted glucose of concentration $C_2 = 0.95\ mg/ml$. Following the same recipe, the last concentration C_3 was composed by adding a third drop of volume ($V_3 \approx 0.1\ mL$) of distilled water of 0 mg/ml resulting into $0.3\ mL$ glucose sample inside the container with a new concentration of $C_3 = 0.63\ mg/ml$. In each trial, measurements were recorded for changes in the Q-factor at the WGH_{700} resonance mode at $f = 53.7\ GHz$ as shown in Fig. 22.

The resolution of the resonant amplitude variations against the glucose concentrations is plotted in the enclosed window inside Fig. 22. Other WGH modes exhibit similar behavior in changing the resonance amplitudes but with lower resolutions. Interestingly, in all the cases of loaded glucose samples it was observed that the WGH resonances exhibit higher Q-factors as compared with the no-sample case (solid blue). This is because of the increased attenuation loss inside the resonator resulted from the added delicate layer of glucose sample, as a result the coupling state tends closer to the critical coupling condition. These perturbations observed in the last experiments are considerably dominant by the amount of loss that varies from one tested concentration to another. To prove this experimentally, we repeated the following tests of adding one drop of $V \approx 0.1\ mL$ and $C = 1.2\ mg/ml$ inside the container and recorded a reading of approximately -11.30 dB for the transmission coefficient at $f = 53.63\ GHz$

resonant frequency of WGH_{700}. Another drop of the same volume and concentration was added inside the container, and no significant change was noticed in the recorded reading. The test was repeated using a sample of different concentration $C = 1.1\ mg/ml$ which was added twice inside the container with no change in the recorded $|S_{21}|$ of about -13.8 dB at $f = 53.7\ GHz$. However, a considerable jump in $|S_{21}|$ was noticed in the third trial when two droplets of different concentrations $C = 0$ and $1.2\ mg/ml$ were added respectively inside the container causing the $|S_{21}|$ to jump from -18.2 dB to -17.4 dB at $f = 50.13\ GHz$ of the WGH_{600} mode.

To achieve accurate producible measurements, we ensured that our mm-wave regime was calibrated precisely to limit the measurement error due to transmission loss to less than 0.02 dB over the entire frequency range. Moreover, all the glucose sensing experiments were held in an environment of controlled and monitored temperature to reduce the environmental impact on the collected scattering data. Particularly, the temperature in the experimentation room was regulated at 22 ± 1°C. However, the resonance characteristics of the integrated sensor would not be considerably affected by such small fluctuation in temperature (less than ±2 MHz shift in the resonance frequency) as both alumina and silicon have low thermal expansion coefficients. In addition, given the strong dependency of the sensor transmitted mm-waves on the dielectric properties of the tested glucose samples, where those properties are known to be functions of the sample temperature; therefore, all the glucose samples were stored in the same temperature condition of 22 ± 1°C. All the measurements were repeated three times for repeatability verifications while making sure to exactly retrieve the initial resonance response of the unloaded DDR when the sample container is taken off for cleaning for a new repeatability trial. The error bars are included in the enclosed $|S_{21}|$ measurements in Fig. 22 to indicate a repeatability error of about ±0.03 dB in each reading.

VII. DISCUSSION

With dielectric permittivity measurements investigated in different frequency bands, mm-wave frequency range has shown to be more promising for sensing the glucose-loaded solutions for many reasons: non-ionizing nature, good penetration depths inside the liquid tissues, and the good resolution feature for their relatively small wavelength compared to EM radiations at lower microwave frequencies. In the DAK-TL spectroscopy for glucose-loaded solutions at the mm-wave high frequency range, it is observed that with an increased concentration of glucose content in watery solutions, the real part of the relative permittivity (i.e. dielectric constant) increases slightly while the loss tangent decreases by a notably large amount (implicit decrease of the imaginary part of relative permittivity and conductivity). When compared against the extracted dielectric properties in lower-frequency bands, it is observed that the difference in dielectric constant and loss tangent between various glucose concentrations is increasing beyond 50 GHz. This would imply a difficulty in detecting the tiny differences between the dielectric properties of the respective glucose samples in the lower frequency ranges. Seemingly, 50–67 GHz is a promising glucose sensing region where a noticeable complex permittivity contrast between various glucose concentrations is evidenced.

As part of this study, we also probed into the DAK-TL accuracy in measurements at different volumes of the tested liquid samples to conclude the lowest volume of liquid that could be used for acquiring stable and precise measurements. In particular, the dielectric properties of standard distilled water were measured in four different frequency bands at different volumes of 10, 5, 3, 2 and 1 mL using two petri-dishes of different capacities. By comparing the collected measurements at each volume against the reference target data provided in the DAK-TL database, measurements on the 10 mL volume were observed to be relatively close to the exact data of distilled water while other volumes were slightly off. In that event, all the dielectric measurements of glucose aqueous solutions were collected using the DAK-TL system at volume $V = 10\ mL$ to desire stable and precise dielectric parameters. The results have also revealed the challenge for testing the samples of smaller volumes at higher frequency bands, that probably need to be repeated multiple times. Besides, it would result into less accurate measurements with few ripples appeared towards higher frequencies (59–66 GHz). Similarly, the influence of the exact touching point between the sensing probe and the tested sample was investigated. Considering that the probe can go to different distances between 0 to 10 mm (at zero distance the probe becomes in touch with the sample platform while at 10 mm distance the probe is fully off), measurements have shown that more accurate results would be achieved if a sample of volume 10 mL for example is tested at a probe distant of 4 mm that would yield a sufficient contact compared to the 3 mm case where the probe immerses deeper inside the liquid.

The proposed WGM sensor was designed to work in the mm-wave frequency range 50–70 GHz aiming at the accurate detection of the glucose levels resembling the normal diabetes condition. The proposed bio-sensor achieved higher levels of sensitivity when the lower order modes WGH_{600} and WGH_{700} were excited inside the resonator. This is explained by their longer evanescent field tails that enable the spread of the coupled electric-field at higher magnitudes inside the glucose samples compared to those of WGH_{800} and WGH_{900} where the fields are more concentrated towards the boundary. These higher order modes might prove a leverage for different sample allocations, for example placing small droplets in the boundary of the DDR, which is impractical for continuous glucose monitoring purpose.

In this study, we adopted one measure of the sensitivity as calculated from the variations in the transmission resonant amplitudes at each WGH mode. However, from theoretical perspectives the variations on the glucose levels could also be tracked on the transmission phases near resonances as demonstrated by the numerical simulations in a previous

TABLE 5. Comparison against other state-of-the-art sensors for glucose level detection.

Ref	Sample volume (μL)	Concentration (mg/ml)	Operating frequency (GHz)	Sensing parameter	S (dB per mg/ml)
[39]	7500	0.78 – 50	1.4 – 1.9	$\|S_{11}\|$	0.18
[40]	-	0 – 4	2.4 – 2.9	$\|S_{21}\|$	0.0075
[41]	-	0 – 3	60 – 80	$\|S_{21}\|$	0.23
[42]	-	0.3 – 80	7.5	$\|S_{21}\|$	0.008
[43]	170	5 – 25	1.91	$\|S_{21}\|$	0.025
[44]	20	40 – 200	2.5 – 6	$\|S_{21}\|$	0.01
[26]	-	5 – 50	14-16	Phase	0.02°
[45]	20	200 – 1000	3.02	$\|S_{21}\|$	0.007
[46]	1000	0 – 300	2.0 – 2.5	$\|S_{11}\|$	0.003
This work	50 – 370	0.7 – 1.2	50 – 70 GHz (WGM modes)	$\|S_{21}\|$	0.8 – 1 (Measurement) 2.5 – 7.7 (Simulation)

discussion. These variations in the transmission phase responses were also observed in the practical measurements using the preliminary sensor prototype but they did not change significantly from one concentration to another. This is because the fabricated sensor was not optimized for the highest sensitivity in terms of the critical coupling gap. However, the level of sensitivity recorded experimentally at one mode WGH_{700} has shown to be much higher compared to other glucose sensors operating at different frequency bands and recently reported in the literature as shown in Table 5. For instance, the Microstrip line (MLIN)-based glucose sensor proposed in [39] achieved an average sensitivity of 0.18 dB/(mg/ml) in terms of the reflection coefficient when working in the frequency band 1.4–1.9 GHz. The sensor exploits the interaction between the main field and the SUT in the substrate region of an MLIN terminated with a load. The fluidic glucose sensor proposed in [40] used a complementary split-ring resonator (CSRR) in the frequency band 2.4–2.9 GHz was able to detect 0.03 dB variation in $|S_{21}|$ when the glucose level changed from 0 to 4 mg/ml (i.e. sensitivity of 0.0075 dB/(mg/ml)). The work in [41] used a setup of a VNA connected to two horn antennas to sense glucose samples inside a plastic liquid container in the mm-wave range 60–80 GHz. Collected measurements recorded 0.7 dB as the largest change in the transmission magnitude for the variation from 0 to 3 mg/ml at some frequency points (i.e. sensitivity of 0.23 dB/(mg/ml)). However, our proposed WGM sensor realizes a minimum of 0.8–1 dB/(mg/ml) measured sensitivity when operating at the WGH_{700} mode. This is demonstrated by measuring the transmission responses for the WGH_{700} to glucose changes under non-critical coupling condition. The WGH_{600} (below 50 GHz) would likely achieve a higher measure as evidenced by the numerical simulations. In addition, the sensor can be optimized in terms of the DIG-to-DDR gap to trigger the critical coupling state for these lower order modes and thereby acquire higher sensitivity similar to those calculated from the optimized simulations 2.5–7.7 dB/(mg/ml). Furthermore, the WGM sensor with the curved DIG is also expected to score higher in this field as evidenced by the finite element simulations.

VIII. CONCLUSION

Towards the purpose of developing a non-invasive glucose monitoring sensor for diabetics, in this paper we investigated the dielectric properties of diabetes-resembling aqueous samples of small concentrations (0.7–1.2 mg/ml) through measurements using a commercial coaxial kit (DAK-TL) in the broad band 300 MHz–67 GHz. The mm-wave range 50–67 GHz has shown to be promising for differentiating between glucose samples of lossy characteristics as demonstrated by the noticeable trend among various concentrations and the amount of change in dielectric constant and loss tangent due to varying glucose level. Using this finding, an integrated low-cost mm-wave WGM sensor of simple structure is proposed as a sensing platform for a continuous glucose level detection. The sensor exploits the intensified WGM fields launched towards the boundaries of a DDR via an Alumina-made image waveguide to detect small variations in the dielectric properties of the loaded samples of small glucose concentrations. It is shown theoretically, numerically and experimentally that WGM travelling-waves at mm wavelengths are quite sensitive to perturbations in the loss property of the integrated sensor when the glucose level is changed. The sensor achieves a high level of sensitivity when the lower order modes WGH_{600} and WGH_{700} are excited inside the resonator with a superiority performance for the curved-DIG as demonstrated by numerical simulations in the mm-wave band. A concentration difference as small as 0.1 mg/ml can be easily resolved using a preliminary prototype of the proposed WGM sensor that employs a straight-DIG as evidenced by the in-lab measurements using a convenient setup.

REFERENCES

[1] M. Zhadobov, N. Chahat, R. Sauleau, C. Le Quement, and Y. Le Drean, "Millimeter-wave interactions with the human body: State of knowledge and recent advances," *Int. J. Microw. Wireless technol.*, vol. 3, no. 2, pp. 237–247, Mar. 2011.

[2] M. Abidi, A. Elhawil, J. Stiens, R. Vounchx, J. B. Tahar, and F. Choubani, "Sensing liquid properties using split-ring resonator in mm-wave band," in *Proc. IECON - 36th Annu. Conf. IEEE Ind. Electron. Soc.*, Glendale, AZ, USA, Nov. 2010, pp. 1298–1301.

[3] A. D. Association, "Diagnosis and classification of diabetesmellitus," *Diabetes Care*, vol. 37, pp. S81–S90, Jan. 2014.

[4] Canadian Diabetes Association. *Self-Monitoring of Blood Glucose*. Accessed: Jan. 12, 2018. [Online]. Available: http://www.diabetes.ca/clinical-practiceeducation/professional-resources/selfmonitoring-of-bloodglucose

[5] H. Cano-Garcia, P. Kosmas, I. Sotiriou, I. Papadopoulos-Kelidis, C. Parini, I. Gouzouasis, G. Palikaras, and E. Kallos, "Detection of glucose variability in saline solutions from transmission and reflection measurements using V-band waveguides," *Meas. Sci. Technol.*, vol. 26, no. 12, Oct. 2015, Art. no. 125701.

[6] D. Cunningham and J. Stenken, *In vivo Glucose Sensing*, Hoboken, NJ, USA: Wiley, 2010.

[7] R. Weiss, Y. Yegorchikov, A. Shusterman, and I. Raz, "Noninvasive continuous glucose monitoring using photoacoustic technology–results from the first 62 subjects," *Diabetes Technol Therapeutics*, vol. 9, no. 1, pp. 68–74, Feb. 2007.

[8] A. Sieg, R. H. Guy, and M. B. Delgado-Charro, "Noninvasive and minimally invasive methods for transdermal glucose monitoring," *Diabetes Technol. Therapeutics*, vol. 7, no. 1, pp. 174–197, Feb. 2005.

[9] O. Amir, D. Weinstein, S. Zilberman, M. Less, D. Perl-Treves, H. Primack, A. Weinstein, E. Gabis, B. Fikhte, and A. Karasik, "Continuous noninvasive glucose monitoring technology based on 'occlusion spectroscopy,'" *J. Diabetes Sci. Technol.*, vol. 1, no. 4, pp. 463–469, Jun. 2016.

[10] S. K. Vashist, "Non-invasive glucose monitoring technology in diabetes management: A review," *Analytica Chim. Acta*, vol. 750, pp. 16–27, Oct. 2012.

[11] S. Malik, S. Gupta, R. Khadgawat, and S. Anand, "A novel non-invasive blood glucose monitoring approach using saliva," in *Proc. IEEE Int. Conf. Signal Process., Informat., Commun. Energy Syst. (SPICES)*, Feb. 2015, pp. 1–5.

[12] W. Gao, S. Emaminejad, H. Y. Y. Nyein, S. Challa, K. Chen, A. Peck, H. M. Fahad, H. Ota, H. Shiraki, D. Kiriya, D.-H. Lien, G. A. Brooks, R. W. Davis, and A. Javey, "Fully integrated wearable sensor arrays for multiplexed *in situ* perspiration analysis," *Nature*, vol. 529, no. 7587, pp. 509–514, Jan. 2016.

[13] J. Zhang, W. Hodge, C. Hutnick, and X. Wang, "Noninvasive diagnostic devices for diabetes through measuring tear glucose," *J. Diabetes Sci. Technol.*, vol. 5, no. 1, pp. 166–172, Jan. 2011.

[14] H. Choi, J. Naylon, S. Luzio, J. Beutler, J. Birchall, C. Martin, and A. Porch, "Design and *in vitro* interference test of microwave noninvasive blood glucose monitoring sensor," *IEEE Trans. Microw. Theory Techn.*, vol. 63, no. 10, pp. 3016–3025, Oct. 2015.

[15] J. Kim, A. Babajanyan, A. Hovsepyan, K. Lee, and B. Friedman, "Microwave dielectric resonator biosensor for aqueous glucose solution," *Rev. Sci. Instrum.*, vol. 79, no. 8, Aug. 2008, Art. no. 086107.

[16] H. Cano-Garcia, I. Gouzouasis, I. Sotiriou, S. Saha, G. Palikaras, P. Kosmas, and E. Kallos, "Reflection and transmission measurements using 60 GHz patch antennas in the presence of animal tissue for non-invasive glucose sensing," in *Proc. 10th Eur. Conf. Antennas Propag. (EuCAP)*, Davos, Switzerland, Apr. 2016, pp. 1–3.

[17] P. H. Siegel, Y. Lee, and V. Pikov, "Millimeter-wave non-invasive monitoring of glucose in anesthetized rats," in *Proc. 39th Int. Conf. Infr., Millim., Terahertz Waves (IRMMW-THz)*, Tucson, AZ, USA, Sep. 2014, pp. 1–2.

[18] M. Hofmann, M. Bloss, R. Weigel, G. Fischer, and D. Kissinger, "Non-invasive glucose monitoring using open electromagnetic waveguides," in *Proc. 42nd Eur. Microw. Conf.*, Amsterdam, The Netherlands, Oct. 2012, pp. 546–549.

[19] P. M. Meaney, A. P. Gregory, J. Seppala, and T. Lahtinen, "Open-ended coaxial dielectric probe effective penetration depth determination," *IEEE Trans. Microw. Theory Techn.*, vol. 64, no. 3, pp. 915–923, Mar. 2016.

[20] H. Yoshikawa and A. Nakayama, "Measurements of complex permittivity at millimeter-wave frequencies with an end-loaded cavity resonator," *IEEE Trans. Microw. Theory Techn.*, vol. 56, no. 8, pp. 2001–2007, Aug. 2008.

[21] D. L. Creedon, Y. Reshitnyk, W. Farr, J. M. Martinis, T. L. Duty, and M. E. Tobar, "High Q-factor sapphire whispering gallery mode microwave resonator at single photon energies and millikelvin temperatures," *Appl. Phys. Lett.*, vol. 98, no. 22, May 2011, Art. no. 222903.

[22] G. Annino, M. Cassettari, I. Longo, and M. Martinelli, "Whispering gallery modes in a dielectric resonator: Characterization at millimeter wavelength," *IEEE Trans. Microw. Theory Techn.*, vol. 45, no. 11, pp. 2025–2034, Nov. 1997.

[23] A. Brady, C. McCabe, and M. McCann, *Fundamentals of Medical Surgical Nursing*. Hoboken, NJ, USA: Wiley, 2013.

[24] K. Yaws, D. Mixon, and W. Roach, "Electromagnetic properties of tissue in the optical region," *Proc. SPIE Int. Soc. for Opt. Photon. Biomed. Opt.*, vol. 6435, Feb. 2007, Art. no. 643507.

[25] V. Komarov, S. Wang, and J. Tang, *Permittivity and Measurements*. Hoboken, NJ, USA: Wiley, 2005, doi: 10.1002/0471654507.eme308.

[26] M. Hofmann, G. Fischer, R. Weigel, and D. Kissinger, "Microwave-based noninvasive concentration measurements for biomedical applications," *IEEE Trans. Microw. Theory Techn.*, vol. 61, no. 5, pp. 2195–2204, May 2013.

[27] V. V. Meriakri, E. E. Chigrai, I. P. Nikitin, and M. P. Parkhomenko, "Dielectric properties of water solutions with small content of glucose in the millimeter–wave band and the determination of glucose in blood," in *Proc. Int. Kharkiv Symp. Phys. Engrg. Millim. Sub-Millimeter Waves (MSMW)*, Kharkov, Ukraine, Jun. 2007, pp. 873–875.

[28] V. V. Meriakri, E. E. Chigrai, D. Kim, I. P. Nikitin, L. I. Pangonis, M. P. Parkhomenko, and J. H. Won, "Dielectric properties of glucose solutions in the millimetre-wave range and control of glucose content in blood," *Meas. Sci. Technol.*, vol. 18, no. 4, pp. 977–982, Feb. 2007.

[29] S. Saha, H. Cano-Garcia, I. Sotiriou, O. Lipscombe, I. Gouzouasis, M. Koutsoupidou, G. Palikaras, R. Mackenzie, T. Reeve, P. Kosmas, and E. Kallos, "A glucose sensing system based on transmission measurements at millimetre waves using micro strip patch antennas," *Sci. Rep.*, vol. 7, no. 1, pp. 1–11, Jul. 2017.

[30] A. E. Omer, G. Shaker, S. Safavi-Naeini, K. Murray, and R. Hughson, "Glucose levels detection using mm-wave radar," *IEEE Sensors Lett.*, vol. 2, no. 3, pp. 1–4, Sep. 2018.

[31] J. Baker-Jarvis, M. D. Janezic, P. D. Domich, and R. G. Geyer, "Analysis of an open-ended coaxial probe with lift-off for nondestructive testing," *IEEE Trans. Instrum. Meas.*, vol. 43, no. 5, pp. 711–718, Oct. 1994.

[32] V. Turgul and I. Kale, "On the accuracy of complex permittivity model of glucose/water solutions for non-invasive microwave blood glucose sensing," in *Proc. E-Health Bioeng. Conf. (EHB)*, Iasi, Nov. 2015, pp. 1–4.

[33] T. Karacolak, E. C. Moreland, and E. Topsakal, "Cole-cole model for glucose-dependent dielectric properties of blood plasma for continuous glucose monitoring," *Microw. Opt. Technol. Lett.*, vol. 55, no. 5, pp. 1160–1164, Mar. 2013.

[34] M. Hofmann, F. Trenz, R. Weigel, G. Fischer, and D. Kissinger, "A microwave sensing system for aqueous concentration measurements based on a microwave reflectometer," in *IEEE MTT-S Int. Microw. Symp. Dig.*, Montreal, QC, Canada, Jun. 2012, pp. 1–3.

[35] D. Cros and P. Guillon, "Whispering gallery dielectric resonator modes for W-band devices," *IEEE Trans. Microw. Theory Techn.*, vol. 38, no. 11, pp. 1667–1674, Nov. 1990.

[36] X. Hu Jiao, P. Guillon, L. A. Bermudez, and P. Auxemery, "Whispering-gallery modes of dielectric structures: Applications to millimeter-wave bandstop filters," *IEEE Trans. Microw. Theory Techn.*, vol. 35, no. 12, pp. 1169–1175, Dec. 1987.

[37] G. Annino, M. Cassettari, and M. Martinelli, "Study on planar whispering gallery dielectric resonators. I. General properties," *Int. J. Infr. Millim. Waves*, vol. 23, no. 4, pp. 597–615, 2002.

[38] M. Neshat, H. Chen, S. Gigoyan, D. Saeedkia, and S. Safavi-Naeini, "Whispering-gallery-mode resonance sensor for dielectric sensing of drug tablets," *Meas. Sci. Technol.*, vol. 21, no. 1, Nov. 2009, Art. no. 015202.

[39] S. Y. Huang, Omkar, Y. Yoshida, A. J. G. Inda, C. X. Xavier, W. C. Mu, Y. S. Meng, and W. Yu, "Microstrip line-based glucose sensor for noninvasive continuous monitoring using the main field for sensing and multivariable crosschecking," *IEEE Sensors J.*, vol. 19, no. 2, pp. 535–547, Jan. 2019.

[40] C. Jang, J.-K. Park, H.-J. Lee, G.-H. Yun, and J.-G. Yook, "Temperature-corrected fluidic glucose sensor based on microwave resonator," *Sensors*, vol. 18, no. 11, p. 3850, Nov. 2018.

[41] S. Hu, S. Nagae, and A. Hirose, "Millimeter-wave adaptive glucose concentration estimation with complex-valued neural networks," *IEEE Trans. Biomed. Eng.*, vol. 66, no. 7, pp. 2065–2071, Jul. 2019.

[42] T. Chretiennot, D. Dubuc, and K. Grenier, "Microwave-based microfluidic sensor for non-destructive and quantitative glucose monitoring in aqueous solution," *Sensors*, vol. 16, no. 10, p. 1733, Oct. 2016.

[43] G. Gennarelli, S. Romeo, M. R. Scarfi, and F. Soldovieri, "A microwave resonant sensor for concentration measurements of liquid solutions," *IEEE Sensors J.*, vol. 13, no. 5, pp. 1857–1864, May 2013.

[44] S. Harnsoongnoen and A. Wanthong, "Coplanar waveguide transmission line loaded with electric-LC resonator for determination of glucose concentration sensing," *IEEE Sensors J.*, vol. 17, no. 6, pp. 1635–1640, Mar. 2017.

[45] S. Harnsoongnoen and A. Wanthong, "Coplanar waveguides loaded with a split ring resonator-based microwave sensor for aqueous sucrose solutions," *Meas. Sci. Technol.*, vol. 27, no. 1, Dec. 2015, Art. no. 015103.

[46] S. Kim, J. Kim, A. Babajanyan, K. Lee, and B. Friedman, "Noncontact characterization of glucose by a waveguide microwave probe," *Current Appl. Phys.*, vol. 9, no. 4, pp. 856–860, Jul. 2009.

ALA ELDIN OMER (Student Member, IEEE) received the primary and secondary education in Khartoum, Sudan. He was ranked as the third top student over whole Sudan ranking in the Sudanese High School Certificate (SHSC) with an average of (96.4%). He received the B.Sc. degree *(magna cum laude)* in electrical and electronics engineering with specialization in communication engineering from the University of Khartoum, Sudan, in 2013, the M.Sc. degree *(summa cum laude)* in electrical engineering from the American University of Sharjah (AUS), in 2016, where he was awarded a two-year Graduate Assistantship from the Department of Electrical Engineering. He is currently pursuing the Ph.D. degree with the Centre for Intelligent Antenna and Radio Systems (CIARS), Department of Electrical and Computer Engineering, University of Waterloo, Canada. During his Ph.D., he has been a Visiting Research Assistant with the Electronics and Electromagnetism Laboratory (L2E), Sorbonne University. From 2013 to 2014, he was a Research and Development Communication Engineer with the Telecommunication Research Centre (TRC) part of GIAD Industrial Group Company, Khartoum. In addition, since 2014, he has also been a Teaching and Research Assistant with the Department of Electrical Engineering, AUS. He has coauthored number of journal and conference papers presented in international conferences. His research interests include communication systems, cognitive radio networks, video streaming, micro/mm-wave sensing, bio-sensors, bio-electromagnetics, complex propagation and scattering phenomena, radar systems, signal processing, and pattern classification. He has been awarded many prestigious awards, Singapore International Pre-Graduate Award (SIPGA), the IEEE Antennas and Propagation Society Doctoral Research Grant, NSERC CREATE fellowship, Erasmus+ mobility grant, and the University of Waterloo Faculty of Engineering (FOE) awards.

SUREN GIGOYAN received the M.S. degree from the Department of Physics, Yerevan State University, Yerevan, Armenia, in 1980, and the Ph.D. degree in electrical engineering from the Institute of Electrical Engineering, Moscow, Russia, in 1991. From 2005 to 2006, he was a Visiting Fulbright Scholar with the University of Tennessee, Knoxville, TN, USA. He is currently a Visitor Scientist with the Centre for Intelligent Antenna and Radio System, University of Waterloo, Waterloo, ON, Canada. He has authored/coauthored more than 70 peer-reviewed journal and conference papers. His current research interests include millimeter and THz spectroscopy, submillimeter frequency range devices and system design, application of MEMS structures in THz spectroscopy, sensing, cancer, and DNA detection.

GEORGE SHAKER (Senior Member, IEEE) received the B.A.Sc., M.A.Sc., and Ph.D. degrees. From 2006 to 2011, he was with the RIM's (Blackberry's) RF Research and Development Division, first as an NSERC Scholar, then as a Senior EM Researcher, reporting directly to the RIM's Vice President of RF Research and Development. From 2009 to 2010, he was a Visiting NSERC MSFSS Scholar with the Georgia Institute of Technology. He has been an Adjunct Assistant Professor with the Department of Electrical and Computer Engineering, University of Waterloo, since 2014. He has also been with Sparktech Labs (formerly DBJay Ltd.), where he has also been the Principal Scientist and the Head of Electromagnetics Research and Development, since 2011. From 2011 to 2013, he was a Senior Team Member and the Head of Technology of DBJ's Sister Company, China. He was heavily involved in designing a line of compact chambers product and the line of compact chambers for next-generation wireless systems, including MIMO and RFIDs. Over the last decades, he has contributed to products available from Hi-Tek International, Panasonic, ActsPower, COM DEV Ltd., Research in Motion (BlackBerry), American Microelectronic Semiconductors (ON-Semiconductors), Bionym, Medella Health, Novela, DBJ Tech, Konka, Enice, China Mobile, Tri-L Solutions, Pebble, Thalmic Labs, Lyngsoe Systems, NERV, and Spark Tech Labs. He has coauthored two articles in the IEEE SENSORS, which were among the top 25 downloaded articles on the IEEE Xplore for several consecutive months, in 2012 and 2017. He has coauthored over 70 journal publications, conference papers, and technical reports, along with more than 15 patents/patent applications. Dr. Shaker has served as a TPC/TPRC Member of the IEEE MTT-IMS, the IEEE iWAT, the IEEE EMC, the IEEE WF-IoT, the IEEE AP-S, the IEEE EuCAP, and the IEEE iThings. He was an Invited Speaker with several international events, including Keynote talks at the IEEE LAPC, the IEEE iThings, and the Ambient Intelligence. He was a recipient of multiple awards, including the NSERC Canada Graduate Scholarship (sole winner in the area of electromagnetics across Canada, in 2007), the Ontario Graduate Scholarship (twice), the European School of Antennas Grant at IMST GmbH, in 2007, the top 3 IEEE AP-S Best Paper Award, in 2009, the IEEE AP-S Best Paper Award (HM, in 2008, 2011, and 2017), the IEEE Antennas and Propagation Graduate Research Award, from 2008 to 2009, the NSERC CGS-FSS, in 2009, the IEEE MTT-S Graduate Fellowship, in 2009, the Electronic Components and Technology Best of Session Paper Award, in 2010, the Google Soli Alpha, in 2015, and the IEEE AP-S Third Best Student Design Award, in 2016. He has served as the Session Co-Chair and Short Course/Workshop Lecturer in several international scientific conferences. He currently serves as an Associate Editor for the *IET Microwaves, Antennas, and Propagation*.

SAFIEDDIN SAFAVI-NAEINI (Life Fellow, IEEE) received the B.Sc. degree from the University of Tehran, Tehran, Iran, in 1974, and the M.Sc. and Ph.D. degrees from the University of Illinois at Urbana–Champaign, Champaign, IL, USA, in 1975 and 1979, respectively, all in electrical engineering. He is currently a Professor with the Department of Electrical and Computer Engineering, University of Waterloo, Waterloo, ON, Canada, and holds the Natural Science and Engineering Research Council (NSERC)/C-COM Satellite Systems Industrial Research Chair in Intelligent Radio/Antenna and Novel Electromagnetic Media, where he is also the Director of the Centre for Intelligent Antenna and Radio Systems (CIARS). He has authored or coauthored more than 190 journal articles and 400 conference papers in international conferences. He has led several international collaborative research programs with research institutes in Germany, Finland, Japan, China, Sweden, and USA. His current research interests include the wide range of applications of electromagnetic devices and systems including RF/Microwave technologies, smart integrated antennas and radio systems, mmW/terahertz integrated technologies, vehicular communication systems, emerging radio technologies for intelligent transportation systems (ITSs), nano-EM and photonics, EM in health science and pharmaceutical engineering, wireless communications and sensor systems and networks, new EM materials, bio-electromagnetics, biomedical instruments, and computational methods.